Hyperfine Structure of the Metastable $(1s^2 2s 2p)\ ^3P$ States of $_4Be^9$ and the Nuclear Electric Quadrupole Moment*

ARTHUR G. BLACHMAN† AND ALLEN LURIO
IBM Watson Laboratory at Columbia University, New York, New York
(Received 17 August 1966)

The hyperfine structure (hfs) of $_4Be^9 (I=\frac{3}{2})$ in its metastable $(1s^2 2s 2p)\ ^3P_2$ and $^3P_1$ atomic states has been measured by the atomic-beam magnetic-resonance method. The zero-field hfs intervals in the $^3P_2$ state are

$$\Delta\nu(\tfrac{1}{2},\tfrac{3}{2}) = 187.6157 \pm 0.0042 \text{ Mc/sec},$$
$$\Delta\nu(\tfrac{3}{2},\tfrac{5}{2}) = 312.0226 \pm 0.0021 \text{ Mc/sec},$$
$$\Delta\nu(\tfrac{5}{2},\tfrac{7}{2}) = 435.4773 \pm 0.0021 \text{ Mc/sec}.$$

The zero-field hfs intervals in the $^3P_1$ state are

$$\Delta\nu(\tfrac{1}{2},\tfrac{3}{2}) = 202.9529 \pm 0.0015 \text{ Mc/sec},$$
$$\Delta\nu(\tfrac{3}{2},\tfrac{5}{2}) = 354.4365 \pm 0.0027 \text{ Mc/sec}.$$

In order to obtain the dipole and quadrupole coupling constants from the hfs separations, second- and third-order corrections arising from off-diagonal matrix elements of the hyperfine interaction between the ^3P fine-structure levels must be included. The values of the hfs interaction constants before and after second- and third-order corrections are:

Hfs interaction constant	Uncorrected (Mc/sec)	Corrected (Mc/sec)
$A(^3P_2)$	-124.6167 ± 0.0013	-124.5368 ± 0.0017
$B(^3P_2)$	0.781 ± 0.005	1.429 ± 0.008
$A(^3P_1)$	-140.1564 ± 0.0008	-139.373 ± 0.012
$B(^3P_1)$	-3.2363 ± 0.0007	-0.753 ± 0.044

The individual-electron interaction constants, calculated from the corrected values of A and B, are

$$a_s = -460.2 \pm 1.6 \text{ Mc/sec},$$
$$a_{3/2} = -12.65 \pm 0.54 \text{ Mc/sec},$$
$$b_{3/2} = 1.467 \pm 0.042 \text{ Mc/sec}.$$

The reason for the larger error limits in the corrected, compared with the uncorrected, numbers is discussed and the experimental values of a_s and $a_{3/2}$ are compared with theory. Measurements of the magnetic field dependence of the hfs lead to the following estimate for the ^3P fine-structure separations:

$$W(^3P_2) - W(^3P_1) = 71.86 \pm 0.24 \text{ Gc/sec},$$
$$W(^3P_1) - W(^3P_0) = 19.41 \pm 0.19 \text{ Gc/sec}.$$

From the ratio $b_{3/2}/a_{3/2}$ the quadrupole moment, without Sternheimer polarization corrections, is $Q = +0.049 \pm 0.003$ b. Expressions for the third-order corrections to the zero-field hyperfine energies are given, and estimates of the intermediate coupling coefficients c_1 and c_2 are discussed.

I. INTRODUCTION

THE present paper reports the last in a series of experiments[1] to measure the hfs of the long-lived metastable states of the stable Group II elements by the atomic-beam magnetic-resonance method. Beryllium, the lightest of these elements, has a ground-state configuration $(1s)^2(2s)^2\ ^1S_0$, and the only stable isotope Be^9 has a nuclear spin $I=\frac{3}{2}$. The first excited configuration is $(1s)^2 2s 2p$ in which the s and the p electrons can couple to form the $^1P_1$ and the $^3P_{2,1,0}$ fine-structure levels. These levels are shown in Fig. 1. Although the ^3P levels do not obey an interval rule owing to spin-spin and spin-other-orbit interaction, nevertheless the levels are a very good example of Russell-Saunders (RS) coupling in that the Coulomb interaction energy greatly predominates over the magnetic fine-structure interaction energies. In many ways the structure is similar to that of the helium ^3P levels. In the present work we have obtained a 1% determination of the fine-structure separations, and a preci-

* Based on a dissertation submitted by A. G. Blachman to the faculty of the Graduate School of Arts and Science in partial fulfillment of the requirements for the degree of Doctor of Philosophy at New York University.

† Present address: IBM Watson Research Center, Yorktown Heights, New York.

[1] M. N. McDermott and W. L. Lichten, Phys. Rev. **119**, 134 (1960); W. Faust, M. McDermott, and W. Lichten, *ibid.* **120**, 469 (1960); A. Lurio, *ibid.* **126**, 1768 (1962).

sion determination of these separations is being undertaken.

Since the ^3P levels exhibit good Russell-Saunders coupling, all three ^3P levels are metastable because singlet-triplet transitions cannot occur via electric dipole transitions. In addition, transitions from the $^3P_2$ and the $^3P_0$ levels to the ground state are forbidden by the J selection rules. To the extent that the coupling is not pure RS, the $^3P_1$ state mixes with the short-lived $^1P_1$ state and can have a lifetime considerably shorter than the lifetime of the $^3P_2$ and the $^3P_0$ levels. In the experiments to be discussed, no difference was observed between the lifetimes of the $^3P_1$ and the $^3P_2$ states.

The beam of ^3P metastable-state atoms is produced by electron bombardment of a beam of ground-state atoms, and is detected by the ejection of an electron which occurs when a metastable-state atom in the beam strikes a cesium-coated surface and is de-excited.

From the measurement of the $^3P_2$- and $^3P_1$-state hfs, the magnetic dipole and the electric quadrupole interaction constants are obtained. With a knowledge of these interaction constants, the nuclear electric quadrupole moment of Be^9 is obtained and agrees within 10% as determined from both the $^3P_2$ and $^3P_1$ states.

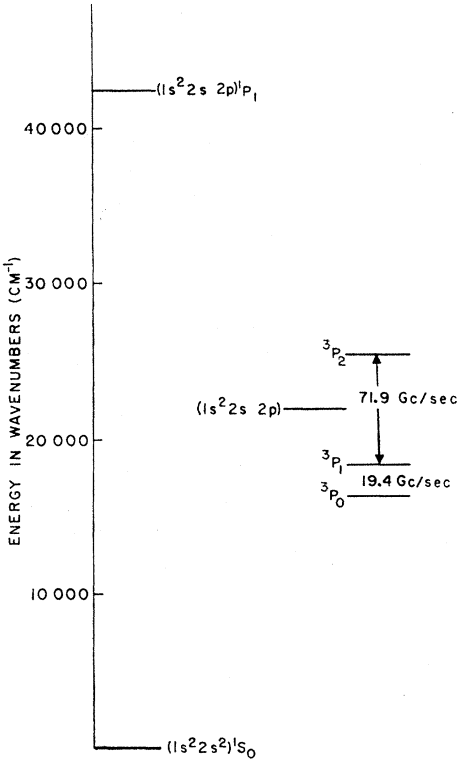

FIG. 1. Energy level diagram of the ground $1s^22s^2\ ^1S_0$ and excited $1s^22s2p\ ^1P$, ^3P states of $_4Be^9$. The separation between the ^3P levels has been expanded relative to the indicated scale.

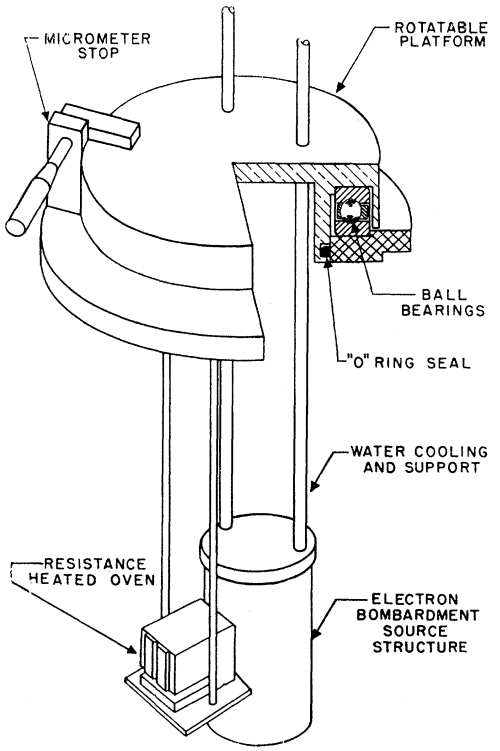

FIG. 2. Rotating oven mount.

II. APPARATUS

The vacuum chamber, magnets and beam geometry used in these measurements are essentially those used by Lurio[1] for hfs measurements on Zn^{67} and Mg^{25}. The primary modifications in the apparatus required for the Be^9 measurements were in the design of the Be source and modifications in the electron bombarder and the detector.

A. Source Ovens

For the purpose of calibrating the magnetic field in the transition region, it is convenient to be able to replace the beryllium beam by a magnesium beam. To facilitate exchanging beams, both ovens are mounted on a common rotating platform. This platform, which is similar to one described by Lew,[2] is shown in Fig. 2. It turns on a roller bearing race and is vacuum sealed by a sliding rubber O-ring.

The Mg oven is the usual resistance-heated oven. The Be source shown in Fig. 3 is a cylindrical oven heated by electron bombardment. Be pellets are placed in a sharp-lipped tungsten crucible (to help prevent creep of molten Be) which sits in a recess in a threaded tantalum pedestal. The tantalum cover which screws onto the pedestal has milled into it a 3-mil wide,

[2] Hin Lew, Phys. Rev. 91, 619 (1953).

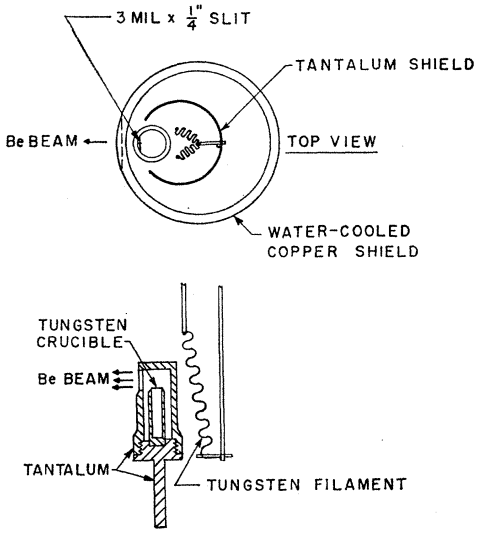

FIG. 3. Electron bombardment source structure.

$\frac{1}{4}$-in. long slit through which the beam emerges. Behind the oven and tilted toward it, so as to be closer at the top of the oven, is the tungsten filament.

Initial problems involving the clogging of the source slit and the flow of the Be onto the outside of the oven were eliminated by constructing the oven so that it is threaded together in a region removed from the slit location and by insuring, through the placement of the filament, that the top, though not necessarily the slit itself, is the hottest part.

The oven temperature is maintained constant by stabilizing the power delivered to the oven. Since the electron-bombardment oven is a thermionic diode in which the oven is the plate, the power delivered to the oven will remain constant if one controls both the voltage and the current in the diode. The voltage is held constant by a regulated power supply. The oven current is regulated by operating the filament in the emission-limited condition and controlling the heating power to the filament. The regulator circuit is patterned after the circuit used in an ion-gauge pressure indicator. The typical operating temperature for the Be oven was about 1525°C as determined by an optical pyrometer reading of the slit temperature. The operating conditions were 750 V and 200 mA. The oven was operated at ground potential since it was found that when it was operated at B^+ potential arcing occasionally occurred between the front of the oven and the water-cooled shield (especially during initial outgassing). To ensure that the emitted electrons go to the oven rather than to other grounded structures, the filament is surrounded in the rear and on the sides by a tantalum shield at the filament potential (see Fig. 3).

B. Bombarder

The bombarder was slightly modified over that used by Lurio.[1] In the present arrangement, the permanent magnet which collimates the vertical beam of electrons is pivoted so that it can be rotated from outside the vacuum system in order to maximize the metastable beam. The heaters in the earlier model, which were used to prevent the bombarder slit from clogging, were omitted since it is not possible to operate the bombarder plate at a temperature hot enough to re-evaporate Be. Also, as a precaution, when the bombarder slit became clogged a chemical cleaning procedure was used since mechanical cleaning of Be-coated surfaces can present a health hazard.

C. Detector

The Auger de-excitation detector for atoms in excited metastable states has been described previously.[1] During the present experiments we used a cesium-coated surface for the detector and found it necessary to evaporate cesium continuously to maintain a detecting surface. A satisfactory cesium spray for coating the surface has been obtained by two methods: (1) from the reaction of cesium chloride with freshly-ground calcium filings in an oven which, after the initial reaction takes place, can be operated at about 250°C; and (2) by evaporation of pure cesium from a Pyrex ampoule inside an oven at about 50°C. The first method has the advantage that the mixture can be exposed to air for some time before loading and can be re-used after the apparatus is exposed to air, provided the exposure time is not long enough for all the Ca to oxidize. In the second method, the cesium can be re-used only if the apparatus is maintained under a good vacuum ($\sim 10^{-6}$ Torr) between heatings of the oven.

The detector is located about 4-in. beyond the beam refocus position and is enclosed, along with the Cs spraying oven and the electrometer, in a liquid-nitrogen-cooled chamber. The detector surface on which the Cs is coated is a brass strip. It is cooled (to make the coating process more efficient) by being connected thermally to the liquid-nitrogen trap with a sapphire rod. Sapphire at 77°K is an excellent thermal conductor and at the same time an electrical insulator. The detection process seems to be independent of the material on which the Cs is sprayed.

III. THEORY OF THE EXPERIMENT AND EXPERIMENTAL PROCEDURE

A. Energy Levels in a Weak Magnetic Field

The energy above the ground state of the ^3P hfs levels in the presence of a weak external magnetic field

is given by

$$W_{F,m_F}(^3P_J)=W_J+\tfrac{1}{2}hA(^3P_J)K+hB(^3P_J)\left[\frac{\frac{3}{4}K(K+1)-I(I+1)J(J+1)}{2I(2I-1)J(2J-1)}\right]+W_F{}^{(2)}(^3P_J)+W_F{}^{(3)}(^3P_J)+m_F g_F\mu_0 H$$
$$+\left[\frac{\alpha^2}{W_F(^3P_J)-W_{F+1}(^3P_J)}+\frac{\beta^2}{W_F(^3P_J)-W_{F-1}(^3P_J)}\right](g_J\mu_0 H)^2, \quad (1)$$

where

$$K\equiv F(F+1)-I(I+1)-J(J+1),$$

and

$$\alpha^2(F-1)=\beta^2(F)=\frac{(F-I+J)(F+I-J)(I+J+1+F)(I+J+1-F)(F^2-m_F{}^2)}{4F^2(2F-1)(2F+1)}.$$

In this expression Planck's constant h is introduced into the second and third terms so that A and B ,the dipole and quadrupole interaction constants, will be in frequency units. The octupole interaction constant C has been omitted since it is negligible within the precision of the present experiments. We have included only the first- and second-order magnetic terms and only the linear term in g_I. Here $W_F{}^{(2)}(^3P_J)$ and $W_F{}^{(3)}(^3P_J)$ are the second- and third-order corrections to the zero-field hfs intervals. These terms must be included because the ratio of the fine structure to the hfs is only about 100 : 1. $W_F{}^{(2)}(^3P_J)$ has been evaluated previously by Lurio, Mandel, and Novick[3] (referred to as LMN) in intermediate coupling. $W_F{}^{(3)}(^3P_J)$ is given in intermediate coupling in Appendix A.

Figures 4 and 5 are schematic drawings of the $^3P_2$

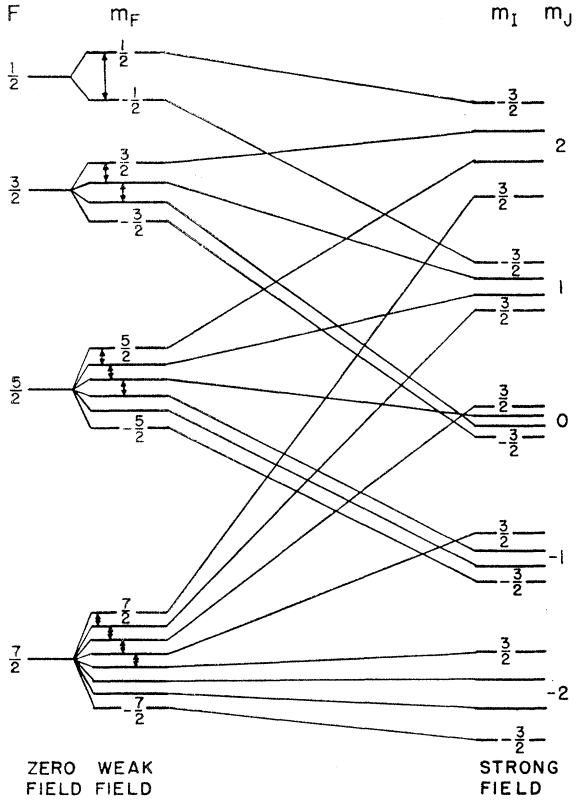

FIG. 4. Schematic drawing of the $^3P_2$ state hfs in weak and strong magnetic field. Observable $\Delta F=0$ transitions are shown by arrowed lines.

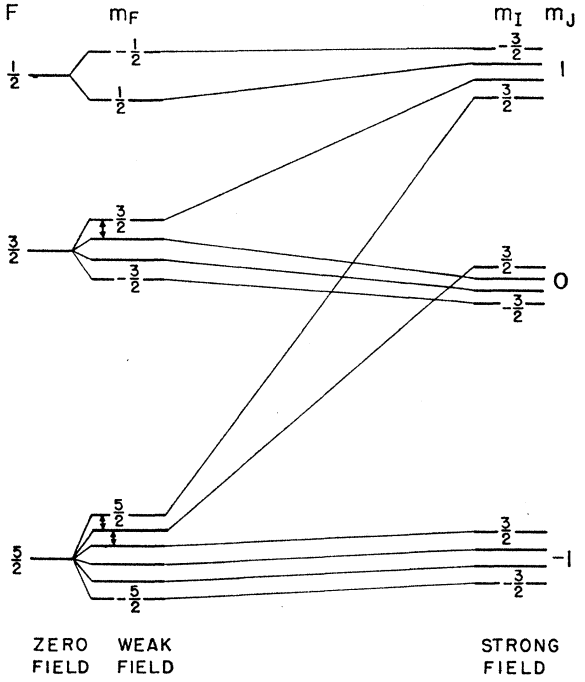

FIG. 5. Schematic drawing of the $^3P_1$ state hfs in weak and strong magnetic field. Observable $\Delta F=0$ transitions are shown by arrowed lines.

[3] A. Lurio, M. Mandel, and R. Novick, Phys. Rev. 126, 1758 (1962): referred to as LMN.

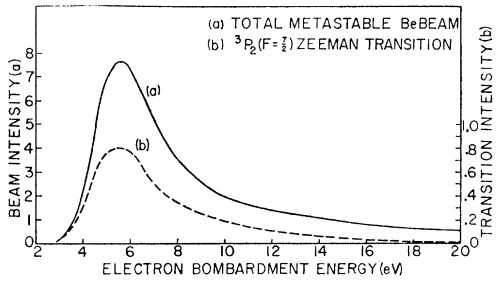

FIG. 6. Excitation curves for the ^3P metastable states of beryllium.

and $^3P_1$ energy levels, respectively, as a function of magnetic field. We have shown the levels in the Paschen-Back region as if the fine structure were much larger than the hfs. This is only a crude approximation for the Be ^3P levels.

B. Verification of the ^3P Metastable States

The only excited states of Be which are expected to be sufficiently metastable to be detected in our apparatus are the $(2s2p)$ ^3P states. Since these states are known[4] to lie 2.725 eV above the ground state, an excitation curve was plotted to check the threshold electron bombardment energy necessary to excite the metastable states. Figure 6 is a graph of the excitation curves obtained for (a) the total metastable Be beam, and (b) the weak-field linear Zeeman transitions, $\Delta F=0$, $\Delta m_F=\pm 1$, in the $F=\frac{7}{2}$ hyperfine level of the $^3P_2$ state. Curve (b) is obtained by taking at each bombardment voltage the difference in beam intensity between rf on and rf off in the transition region. Both curves (a) and (b) have been normalized by dividing the detector signal by the plate current of the electron bombarder since the plate current rises with applied voltage due to space-charge limiting. The maximum refocused beam [at 5.5 eV in curve (a) of Fig. 6] yielded

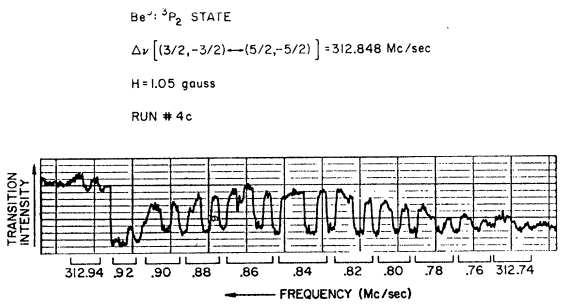

FIG. 7. Recorder trace of the $^3P_2$: $\Delta\nu[(\frac{3}{2},-\frac{3}{2})\leftrightarrow(\frac{5}{2},-\frac{5}{2})]$ transition observed in a magnetic field of 1.05 G. Note that the zero-level of transition intensity shifts throughout this trace. The smooth curve obtained from the above is shown in Fig. 8.

[4] C. E. Moore, *Atomic Energy Levels* (National Bureau of Standards, Washington, D. C., 1949), Vol. I, p. 12; L. Johansson, Arkiv Fysik 23, 119 (1963).

an Auger electron current to the electrometer of about 1.4×10^6 electrons/sec. The peak-to-peak electrometer noise (exclusive of that produced by the Cs coating on the detector surface) in the absence of a beam was equivalent to about 5000 electrons per second.

Two significant features are evident in Fig. 6 which support the identification of the metastable states as the $(2s2p)$ ^3P states. First is the fact that the onset of the observed metastable beam occurs at approximately 2.7 eV; second is the fact that the total metastable beam intensity, curve (a), and that associated with an rf transition, curve (b), have the same shape, indicating that no other metastable states are being detected. The conclusive verification of the states was the observation of all the expected $\Delta F=0$, $\Delta m_F=\pm 1$ transitions at their expected frequencies. In these observations a Mg beam was used to calibrate the magnetic field in the transition region. The measured g_J value for both the $^3P_1$ and the $^3P_2$ states was 1.501 ± 0.001.

C. Zero-Field hfs

An estimate of the zero-field hfs was obtained by measuring the frequencies of certain observable $\Delta F=0$, $\Delta m_F=\pm 1$ transitions in a magnetic field sufficiently large that the individual transitions within a given F state were clearly resolved. From the splitting between these lines and their shift from linear dependence on field, an estimate of the hfs separation may be obtained

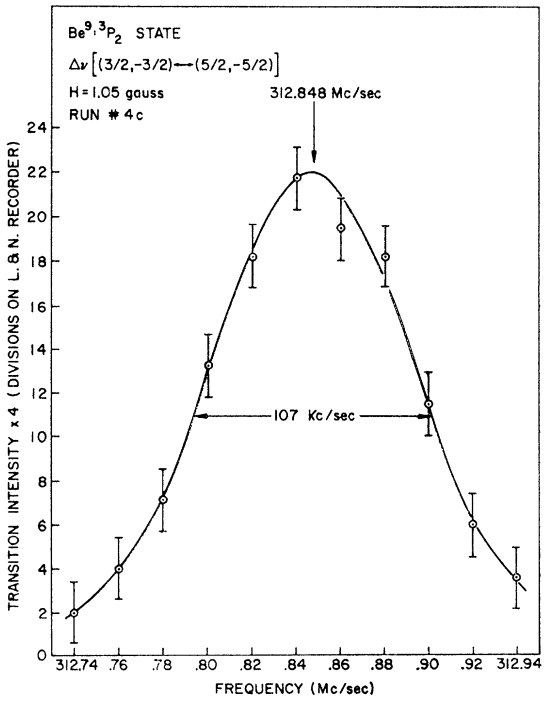

FIG. 8. The $^3P_2$: $\Delta\nu[(\frac{3}{2},-\frac{3}{2})\leftrightarrow(\frac{5}{2},-\frac{5}{2})]$ transition observed in a magnetic field of 1.05 G, obtained from the recorder trace of Fig. 7. Corrected to $H=0$, this curve gives $^3P_2$: $\Delta\nu(\frac{3}{2},\frac{5}{2})=312.020$ Mc/sec.

TABLE I. Measurements and analysis of the data used in the determination of the $^3P_2$-state hfs interval $\Delta\nu(\frac{1}{2},\frac{3}{2})$.[a]

Run	Field-dependent interval measured	Transition	$g_J\mu_0H/h$ (Mc/sec)	Directly measured hfs frequency (Mc/sec)	Full half-width (kc/sec)	Hfs frequency corrected to $H=0$ $\Delta\nu(\frac{1}{2},\frac{3}{2})$ (Mc/sec)	Deviation from the mean (Mc/sec)
1c	$\nu(\frac{1}{2},-\frac{1}{2})-\nu(\frac{3}{2},-\frac{3}{2})=$	π	2.042	188.040	105.4	187.617	0.0013
2c	$\Delta\nu(\frac{1}{2},\frac{3}{2})+0.2\left(\frac{g_J\mu_0H}{h}\right)$	π	2.083	188.055	98.7	187.623	0.0073
3c	$+0.003535\left(\frac{g_J\mu_0H}{h}\right)^2$	π	2.142	188.065	119.9	187.621	0.0053
4c		π	2.072	188.044	121.8	187.614	−0.0017
5a	$\nu(\frac{1}{2},\frac{1}{2})-\nu(\frac{3}{2},\frac{1}{2})=$	σ	1.6894	188.6546	93.4	187.6183	0.0026
6a	$\Delta\nu(\frac{1}{2},\frac{3}{2})+0.6\left(\frac{g_J\mu_0H}{h}\right)$	σ	0.2725	187.774	77.0	187.6099	−0.0058
7a	$+0.007968\left(\frac{g_J\mu_0H}{h}\right)^2$	σ	0.4758	187.900	95.5	187.6127	−0.0030
5b	$\nu(\frac{1}{2},-\frac{1}{2})-\nu(\frac{3}{2},-\frac{1}{2})=$	σ	1.6894	186.6273	109.4	187.6182	0.0025
6b	$\Delta\nu(\frac{1}{2},\frac{3}{2})-0.6\left(\frac{g_J\mu_0H}{h}\right)$	σ	0.2725	187.447	80.0	187.6099	−0.0058
7b	$+0.007968\left(\frac{g_J\mu_0H}{h}\right)^2$	σ	0.4758	187.329	79.5	187.6127	−0.0030

[a] Mean $=\langle\Delta\nu(\frac{1}{2},\frac{3}{2})\rangle=187.6157$ Mc/sec. Standard deviation of the mean $=\pm0.0014$ Mc/sec.

(see Eq. 1). When these estimates had been made, a direct search for the $\Delta F=1$ transitions was undertaken. In this search the signal-to-noise ratio was improved by setting the magnetic field in the transition region so low that all the $\Delta F=1$ $\Delta m_F=0$, ±1, transitions overlapped. In this manner all the hfs transitions were found. Precision measurements of the zero-field hfs were obtained by observing individual $\Delta F=1$ transitions in a weak magnetic field sufficient to resolve all overlaps. The transition intensity at a fixed setting of the rf oscillator was obtained by taking the difference between the detector signal with rf on and with rf off, four times. Figure 7 shows the data as obtained on the recorder for the $^3P_2:\Delta\nu[(\frac{3}{2},-\frac{3}{2})\leftrightarrow(\frac{5}{2},-\frac{5}{2})]$ transition. The smooth curve of transition intensity versus frequency, obtained from Fig. 7, is shown in Fig. 8.

D. Estimate of the ^3P Fine Structure

The Be fine structure separations (see Fig. 1) correspond to transition frequencies in the microwave region. We plan to measure these separations directly in a later experiment. A 1% estimate of these separations is necessary both for planning the direct measurement and for interpreting the present hfs measurements. We have obtained this estimate from the measurements of several hfs transitions at fields of between about 100 and 250 G (see Table II). The

TABLE II. Intermediate magnetic-field hfs measurements.

State	Transition	$\Delta\nu$ (Mc/sec)	μ_0H/h (Mc/sec)	Element used in calibrating magnetic field
$^3P_1$	$(\frac{1}{2},-\frac{1}{2})\leftrightarrow(\frac{3}{2},-\frac{3}{2})$	736.871(18)	366.459(16)	Ar
$^3P_1$	$(\frac{3}{2},-\frac{1}{2})\leftrightarrow(\frac{5}{2},-\frac{3}{2})$	588.008(25)	269.970(15)	Ar
		461.242(15)	149.917(15)	Mg
$^3P_1$	$(\frac{3}{2},-\frac{3}{2})\leftrightarrow(\frac{5}{2},-\frac{5}{2})$	682.725(20)	269.970(15)	Ar
		521.839(15)	149.917(15)	Mg
		521.805(15)	149.898(13)	Mg
		452.563(10)	93.210(10)	Mg
		422.232(15)	66.573(10)	Mg
		400.742(10)	46.724(10)	Mg
		386.392(10)	32.905(10)	Mg
$^3P_2$	$(\frac{5}{2},-\frac{5}{2})\leftrightarrow(\frac{7}{2},-\frac{3}{2})$	352.532(15)	149.917(15)	Mg
		352.533(15)	149.898(13)	Mg
$^3P_2$	$(\frac{5}{2},-\frac{5}{2})\leftrightarrow(\frac{7}{2},-\frac{7}{2})$	696.800(20)	269.970(15)	Ar
		561.114(15)	149.917(15)	Mg

magnitudes of the fine structure separations are such that the measurements between the $^3P_1$-state hfs levels are most sensitive to $W(^3P_1)-W(^3P_0)$, while those between the $^3P_2$-state hfs levels are most sensitive to $W(^3P_2)-W(^3P_1)$. The magnetic field in the transition region for $\mu_0 H/h \leq 150$ Mc/sec was calibrated by measuring the frequency of the nearly degenerate $\Delta m=\pm 1$ transitions in the $^3P_2$ and $^3P_1$ states of the zero nuclear-spin isotopes of Mg. In these measurements we have taken the average value $g_J(\mathrm{Mg})=1.50114$, where an allowance has been made for the diamagnetic and relativistic corrections by the method of Abragam and Van Vleck.[5] In order to remove any possible uncertainty due to our theoretical estimate of $g_J(\mathrm{Mg})$ we calibrated the higher magnetic field measurements by using the $\Delta m=\pm 1$ transitions in the argon $^3P_2$ state whose g_J value has been measured[6] with great precision by comparison with the g_J of hydrogen. A computer diagonalization program was necessary to interpret these results and will be described in Sec. V.

IV. RESULTS

The hfs measurements for the transition $^3P_2$: $\Delta\nu(\frac{1}{2},\frac{3}{2})$ and our method of data reduction are presented in Table I. Here the notation for the zero-field intervals is $\Delta\nu(F,F+1)$. From similar data reduction for the other hfs transitions, we have obtained the following results for the zero-field hfs intervals:

$$^3P_2\begin{cases}\Delta\nu(\frac{1}{2},\frac{3}{2})=187.6157\pm 0.0042 \text{ Mc/sec},\\ \Delta\nu(\frac{3}{2},\frac{5}{2})=312.0226\pm 0.0021 \text{ Mc/sec},\\ \Delta\nu(\frac{5}{2},\frac{7}{2})=435.4773\pm 0.0021 \text{ Mc/sec},\end{cases} \tag{2}$$

$$^3P_1\begin{cases}\Delta\nu(\frac{1}{2},\frac{3}{2})=202.9529\pm 0.0015 \text{ Mc/sec},\\ \Delta\nu(\frac{3}{2},\frac{5}{2})=354.4365\pm 0.0027 \text{ Mc/sec}.\end{cases} \tag{3}$$

The quoted errors are three times the standard deviation of the mean of all runs on a given interval. The weighting of the different observations was based on line symmetry and signal-to-noise considerations.

In Table II are summarized the intermediate magnetic field hfs measurements. These data were taken in order to estimate the ^3P fine structure.

V. DISCUSSION OF RESULTS

A. Calculation of the hfs Interaction Constants

From Eq. (1) we obtain the following theoretical expressions for the zero-field hfs separations in the $^3P_2$ state:

$$\begin{aligned}
\Delta\nu(\tfrac{1}{2},\tfrac{3}{2})&=-\tfrac{3}{2}A(^3P_2)+\tfrac{7}{8}B(^3P_2)+\frac{1}{h}[W_{1/2}{}^{(2)}-W_{3/2}{}^{(2)}+W_{1/2}{}^{(3)}-W_{3/2}{}^{(3)}]_{J=2},\\
\Delta\nu(\tfrac{3}{2},\tfrac{5}{2})&=-\tfrac{5}{2}A(^3P_2)+\tfrac{5}{8}B(^3P_2)+\frac{1}{h}[W_{3/2}{}^{(2)}-W_{5/2}{}^{(2)}+W_{3/2}{}^{(3)}-W_{5/2}{}^{(3)}]_{J=2},\\
\Delta\nu(\tfrac{5}{2},\tfrac{7}{2})&=-\tfrac{7}{2}A(^3P_2)-\tfrac{7}{8}B(^3P_2)+\frac{1}{h}[W_{5/2}{}^{(2)}-W_{7/2}{}^{(2)}+W_{5/2}{}^{(3)}-W_{7/2}{}^{(3)}]_{J=2}.
\end{aligned} \tag{4}$$

For the zero-field hfs separations in the $^3P_1$ state we obtain

$$\begin{aligned}
\Delta\nu\left(\frac{1}{2},\frac{3}{2}\right)&=-\frac{3}{2}A(^3P_1)+\frac{9}{4}B(^3P_1)+\frac{1}{h}[W_{1/2}{}^{(2)}-W_{3/2}{}^{(2)}+W_{1/2}{}^{(3)}-W_{3/2}{}^{(3)}]_{J=1},\\
\Delta\nu\left(\frac{3}{2},\frac{5}{2}\right)&=-\frac{5}{2}A(^3P_1)-\frac{5}{4}B(^3P_1)+\frac{1}{h}[W_{3/2}{}^{(2)}-W_{5/2}{}^{(2)}+W_{3/2}{}^{(3)}-W_{5/2}{}^{(3)}]_{J=1}.
\end{aligned} \tag{5}$$

To obtain the uncorrected values of the hfs interaction constants, we ignore the second- and third-order energy corrections (the bracketed terms) and solve for A and B with the values of $\Delta\nu$ given in Eqs. (2) and (3). Since for the $^3P_2$ state there are three intervals to be fitted by two parameters, we have made a least-squares determination of $A(^3P_2)$ and $B(^3P_2)$. The results of these solutions are given in Table III under the column titled "Uncorrected" interaction constants. If we had included the octupole interaction constant C in the equations for the $^3P_2$ state and solved for the interaction constants, we would have obtained $C(^3P_2)=-0.0003$ Mc/sec while $A(^3P_2)$ and $B(^3P_2)$ would have remained essentially unchanged. The corrected hfs interaction constants listed in the third column of Table III are obtained by an iterative process where the second-order corrections are taken from LMN and the third-order corrections are given in Appendix A. The exact parameters used here will not be specified since in B of this section we will describe in more detail the machine calculation of the same quantities. The necessity for making

[5] A. Abragam and J. H. Van Vleck, Phys. Rev. **92**, 1448 (1953).
[6] A. Lurio, G. Weinreich, C. W. Drake, V. W. Hughes, and J. A. White, Phys. Rev. **120**, 153 (1960).

TABLE III. Values of the hfs interaction constants before and after second- and third-order corrections.

Hfs interaction constant	Uncorrected (Mc/sec)	Corrected (Mc/sec)
$A(^3P_2)$	-124.6167 ± 0.0013	-124.5368 ± 0.0017
$B(^3P_2)$	$0.781\ \pm0.005$	$1.429\ \pm0.008$
$A(^3P_1)$	-140.1564 ± 0.0008	$-139.373\ \pm0.012$
$B(^3P_1)$	$-\ 3.2363\pm0.0007$	$-\ 0.753\ \pm0.044$

these corrections becomes evident, however, upon observing that the largest corrections which occur are $W_{3/2}^{(2)}(^3P_1)$ and $W_{3/2}^{(3)}(^3P_1)$ and amount to 4.2 and -0.03 Mc/sec, respectively.

Solving for $C(^3P_2)$ after including the higher order corrections, we find $C\sim5\times10^{-6}$ Mc/sec where this value, as well as the uncorrected value of C, arises from frequency differences which are smaller than the error in the hfs measurements.

B. Individual-Electron hfs Interaction Constants

Breit and Wills,[7] and Casimir[8] have solved the single-configuration two-electron hfs problem in intermediate coupling for the case where one of the electrons is in an s state. All hyperfine and Zeeman matrix elements for this sl configuration are given by LMN. With the notation of LMN, we have for the sp wave functions

$$\begin{aligned}
&\psi(^3P_2)=|(\tfrac{1}{2},\tfrac{3}{2})_2\rangle,\\
&\psi(^3P_1)=c_1|(\tfrac{1}{2},\tfrac{3}{2})_1\rangle+c_2|(\tfrac{1}{2},\tfrac{1}{2})_1\rangle,\\
&\psi(^3P_0)=|(\tfrac{1}{2},\tfrac{1}{2})_0\rangle,\\
&\psi(^1P_1)=c_2|(\tfrac{1}{2},\tfrac{3}{2})_1\rangle-c_1|(\tfrac{1}{2},\tfrac{1}{2})_1\rangle,
\end{aligned}\tag{6}$$

where the functions are written in jj coupling notation and c_1 and c_2 are the intermediate coupling coefficients. The individual-electron hfs interaction constants a_s, $a_{3/2}$, and $b_{3/2}$ are related to A and B for the $^3P_2$ and $^3P_1$ states through the expressions

$$\begin{aligned}
&A(^3P_2)=\tfrac{1}{4}a_s+\tfrac{3}{4}a_{3/2},\\
&A(^3P_1)=\tfrac{1}{2}a_s(c_2^2-\tfrac{1}{2}c_1^2)\\
&\qquad+a_{3/2}(\tfrac{5}{4}c_1^2-\tfrac{5}{16}\sqrt{2}c_1c_2\xi+\tfrac{5}{2}\theta c_2^2),\\
&B(^3P_2)=b_{3/2},\\
&B(^3P_1)=(\tfrac{1}{2}c_1^2-c_1c_2\sqrt{2}\eta)b_{3/2},
\end{aligned}\tag{7}$$

and

$$\begin{aligned}
&a_{1/2}=5\theta a_{3/2}=-\frac{16}{3}\mu_0^2g_I\left\langle\frac{1}{r^3}\right\rangle F_r(j,Z_i),\\
&b_{3/2}=\tfrac{2}{5}e^2Q\left\langle\frac{1}{r^3}\right\rangle R_r'(l,j).
\end{aligned}\tag{8}$$

[7] G. Breit and L. A. Wills, Phys. Rev. **44**, 470 (1933).

[8] H. B. G. Casimir, *On the Interaction between Atomic Nuclei and Electrons* (Teyler's Tweede Genootschap, Haarlem, Holland, 1936).

The constants ξ, η, and θ are given by Schwartz[9] and F_r and R_r' are tabulated by Kopfermann.[10] μ_0 is the Bohr magneton and g_I is the nuclear g factor. For Be, $\xi=1.000056$, $\eta=1.000196$, $\theta=1.000411$, $F_r(j=\frac{3}{2},Z_i=2)=1.0001$, and $R_r'(l=1,\ j=\frac{3}{2})=1.00016$. The coefficients c_1 and c_2 are estimated in Appendix B and allow a small range of possible values.

A computer program was devised in order to calculate the individual hfs constants from the experimental data and performed the following sequence of operations. A set of values for c_1, c_2, $W(^3P_2)-W(^3P_1)$, and $W(^3P_1)-W(^3P_0)$ was chosen. A and B for both fine-structure states were obtained from the hfs separations by a least-squares solution of Eqs. (4) and (5) ignoring the second- and third-order corrections. From these A and B values the individual-electron hfs interaction constants were calculated by making use of Eqs. (7). The higher order corrections were then calculated using the zero-order estimates of a_s, $a_{3/2}$, and $b_{3/2}$. In this calculation, and in the computation of off-diagonal elements for the matrix diagonalization referred to in the next section, we used an averaged

$$b_{3/2}=\frac{1}{2}\left[B(^3P_2)+\frac{B(^3P_1)}{\frac{1}{2}(c_1^2)-c_1c_2\sqrt{2}\eta}\right].$$

These higher order corrections were then included in Eqs. (4) and (5), and the A and B for each state were recalculated. This iteration process was carried out until no change occurred in the calculated values of the interaction constants. All the terms in the energy matrix were then evaluated (see Appendix C). At $H=0$, the matrices were diagonalized and the hfs separations obtained were compared with the experimental ones. In all cases agreement was obtained to within 1 kc/sec. The values of a_s, $a_{3/2}$, and $b_{3/2}$ obtained from the perturbation theory are therefore self consistent but obviously depend on the values of c_1, c_2, $W(^3P_2)-W(^3P_1)$, and $W(^3P_1)-W(^3P_0)$ chosen. The estimate of these fine-structure separations is discussed in the following section.

C. Estimate of the Fine Structure

The fine-structure separations, as mentioned previously, were obtained from the intermediate field Zeeman effect of the hfs. In this calculation we took for the g_J's the following values which were corrected for diamagnetic and relativistic effects by the method of Abragam and Van Vleck:[5] $g_J(^3P_2)=1.501128$ and $g_J(^3P_1)=1.501115$. The nuclear g_I value is known[11] to be $g_I=4.275\times10^{-4}$ referred to the Bohr magneton. With

[9] C. Schwartz, Phys. Rev. **97**, 380 (1955); Phys. Rev. **105**, 173 (1957.

[10] H. Kopfermann, *Nuclear Moments* (Academic Press Inc., New York, 1958), 2nd ed.

[11] I. Lindgren, "Table of Nuclear Spins and Moments" in *Perturbed Angular Correlations* (North Holland Publishing Company, Amsterdam, 1964).

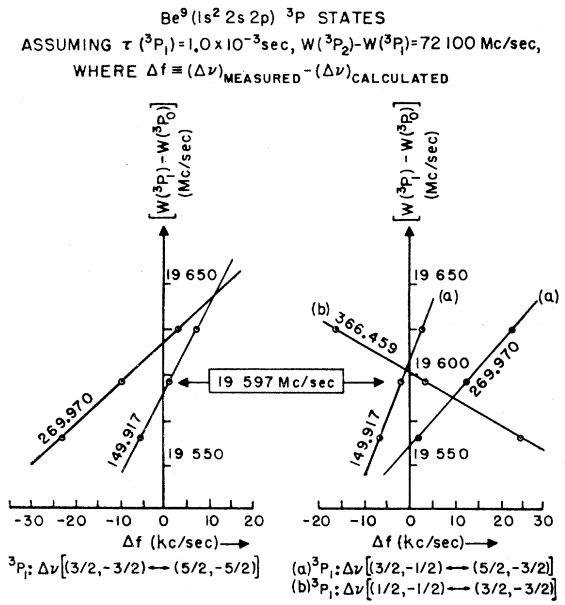

FIG. 9. The above graphs illustrate the method used in estimating the $W(^3P_1)-W(^3P_0)$ fine-structure interval. The ordinate at each circled point is the value of $W(^3P_1)-W(^3P_0)$ assumed in the computer diagonalization program for the value of $(\mu_0 H)/h$ indicated on the curves. The abscissa is the difference between the measured hfs frequency and the predicted hfs frequency. The frequency in the box is the best fit to the data for $\tau(^3P_1)=1.0\times10^{-3}$ sec and $W(^3P_2)-W(^3P_1)=72.1$ Gc/sec.

these parameters, the interaction constants found in the previous section, and the values of H given in Table II, the energy matrices were calculated and diagonalized. The frequencies of the transitions calculated by the computer and those in Table II were compared. By varying the fine-structure energies in the machine program, a "best fit" to these separations could be obobtained. Figure 9 shows how this "best fit" is obtained for $W(^3P_1)-W(^3P_0)$ with $c_1=0.574493$ and $W(^3P_2)-W(^3P_1)=72.10$ Gc/sec. $W(^3P_2)-W(^3P_1)$ was obtained by a similar procedure. In Table IV are given the best fit values of the fine structure and the hfs interaction constants for several values of c_1 and c_2. The spread in these values cannot be reduced until c_1 and c_2 are known more reliably. We therefore have as our final results

$$\begin{aligned} W(^3P_2)-W(^3P_1)&=71.86\pm0.24 \text{ Gc/sec},\\ W(^3P_1)-W(^3P_0)&=19.41\pm0.19 \text{ Gc/sec},\\ a_s&=-460.2\pm1.6 \text{ Mc/sec},\\ a_{3/2}&=-12.65\pm0.54 \text{ Mc/sec}, \end{aligned} \tag{9}$$

and

$$b_{3/2}=1.467\pm0.042 \text{ Mc/sec}.$$

Hartree-Fock (HF) wave functions for the ^3P and ^1P states of Be have been calculated by Hartree and Hartree[12] and by Goodings.[13] Goodings has also calculated the ^3P and ^1P wave functions in the unrestricted Hartree Fock (UHF) approximation. In Table V we compare the individual-electron hfs interaction constants calculated from these wave functions with our experimental values. It can be seen that the value of a_s calculated from Goodings' UHF approximation is in very good agreement with experiment.

TABLE IV. Input parameters and results of machine diagonalization program. The first five rows are values assumed for each calculation. δ is the spread in predicted $^3P_1-{}^3P_0$ fine structure and its smallness is a measure of how well these assumed parameters fit the intermediate field hfs measurements (see Fig. 9). The remaining rows are the results of the calculation. a_0 is the Bohr radius.

$\tau(^3P_1)$ (sec)	∞	1.3×10^{-3}	1.0×10^{-3}
c_1[a]	0.57735	0.57484	0.57449
c_2[a]	0.81650	0.81826	0.81851
$[W(^3P_2)-W(^3P_1)]$ (Mc/sec)	71 630	72 055	72 100
$[W(^3P_1)-W(^3P_0)]$ (Mc/sec)	19 222	19 551	19 597
δ (Mc/sec)	69	60	57
a_s (Mc/sec)	−458.581	−461.426	−461.824
$a_{3/2}$ (Mc/sec)	− 13.189	− 12.240	− 12.107
$b_{3/2}$ (Mc/sec)	1.509	1.436	1.425
$A(^3P_1)$ (Mc/sec)	−139.3841	−139.3639	−139.3610
$B(^3P_1)$ (Mc/sec)	− 0.7964	− 0.7203	− 0.7096
$A(^3P_2)$ (Mc/sec)	−124.5371	−124.5365	−124.5364
$B(^3P_2)$ (Mc/sec)	1.4262	1.4311	1.4319
$B(^3P_2)/B(^3P_1)$ calculated	− 1.7907	− 1.9868	− 2.0178
$B(^3P_2)/B(^3P_1)$ theoretical	− 1.9995	− 1.9995	− 1.9996
$\langle(a_0/r)^3\rangle_{av}$ determined from $a_{3/2}$	0.3302	0.3064	0.3031

[a] These values are based on $\tau(^1P_1)=1.68\times10^{-9}$ sec.

D. Nuclear Electric Quadrupole Moment Q

The p-electron quadrupole interaction constant $b_{3/2}$ may be obtained from either $B(^3P_2)$ or $B(^3P_1)$. Here Q is related to $b_{3/2}$ by the second of Eqs. (8). From Table IV we see that $b_{3/2}$ as obtained from the $^3P_2$ state is very insensitive to the permitted range of intermediate coupling constants and fine structure while the value obtained from the $^3P_1$ state varies by

TABLE V. Comparison of experimental and theoretical values of the individual-electron interaction constants and $\langle(a_0/r)^3\rangle_{av}$.

	Expt.	Hartree & Hartree (HF)	Goodings (HF)	Goodings (UHF)
a_s (Mc/sec)	−460.2	−388.5	−395.0	−454.0
$a_{3/2}$ (Mc/sec)	− 12.65	− 11.24	− 11.79	− 11.79
$\langle(a_0/r)^3\rangle_{av}$	0.317	0.2814	0.2952	0.2951

[12] D. R. Hartree and W. Hartree, Proc. Roy. Soc. London **A154**, 588 (1936).

[13] D. A. Goodings, Phys. Rev. **123**, 1706 (1961).

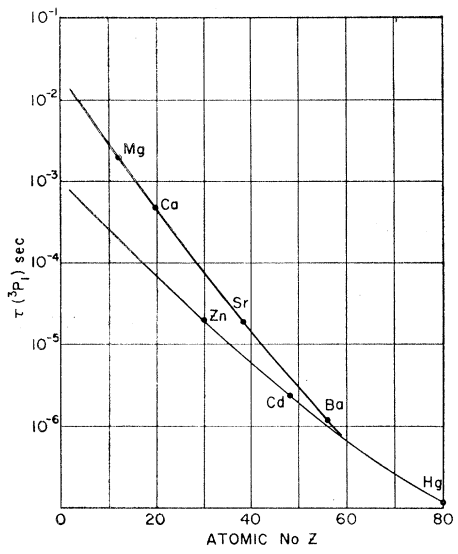

FIG. 10. Measured lifetime of the (sp) $^3P_1$ state of the Group II elements plotted against the atomic number.

as much as 12%. This range of variation in $B(^3P_1)$ is much greater than for the corresponding states in other Group II elements because of the small size of the Be quadrupole interaction energy and the large size of the higher order corrections. We will take, therefore, $b_{3/2}=1.429\pm0.003$ Mc/sec which is the average value of $B(^3P_2)$. The value of $B(^3P_1)$ which is in agreement with the theoretical ratio (ignoring configuration interaction) $B(^3P_2)/B(^3P_1)=-1.9995$ occurs for $\tau(^3P_1)\approx1.2\times10^{-3}$ sec, and this τ agrees rather well with the lifetime expected from extrapolation of the $^3P_1$ lifetimes in the other Group II elements as shown in Fig. 10, Appendix B. $\langle 1/r^3\rangle$ is evaluated from $a_{3/2}$ using the first of Eqs. (8). For Be, one cannot make use of the fine structure for this evaluation since $Z=4$ and the effective atomic number Z_i, which is usually taken to be $Z-4$ (or $Z-n$ where n is the principal quantum number of the p electron[14]), is so arbitrary as to be useless in any calculation. From Eqs. (8) we have

$$\frac{b_{3/2}}{a_{3/2}}=-\frac{3}{8}\frac{e^2QR_r'}{g_I\mu_0^2F_r}=-2.353\times10^{24}Q,$$

where Q is in cm^2. Because of the variation in $a_{3/2}$, Q ranges from 0.0460 to 0.0503 b, but most of the evidence points to a value closer to the latter one at $\tau(^3P_1)=1.0\times10^{-3}$ sec. We therefore quote as our result $Q=+0.049\pm0.003$ b without Sternheimer[15] polarization corrections. This value differs by +0.02 b from our preliminary results.[16]

Note added in proof. A preliminary calculation of the quadrupole shielding factor R for the ^3P state of beryllium has been carried out by Dr. Sternheimer[15,16a] who finds that $R=0.068$. If one applies this correction to the value of $Q_{\text{uncorr.}}$ given in this paper, $Q_{\text{corr.}}=Q_{\text{uncorr.}}/(1-R)=0.0526b$.

A number of theoretical calculations of the Be quadrupole moment have been made. The alpha-particle model yields predictions very close to our experimental result. The most recent calculations, which list earlier work, are by Kunz[17] and by Hiura and Shimodaya.[18]

ACKNOWLEDGMENT

We would like to thank Dr. D. Landman for writing the FORTRAN program for the second- and third-order corrections and for his assistance in some of the zero-field hyperfine structure measurements. We also wish to thank Professor B. Bederson for his interest throughout the course of the work.

APPENDIX A. THIRD-ORDER CORRECTIONS TO THE ZERO-FIELD HYPERFINE ENERGIES

$W_F^{(3)}(^3P_J)$ is the third-order perturbation-theory correction to the hyperfine energy for the ^3P_J state of an sp configuration. With $\mathcal{H}_h$ as defined by LMN and the general-perturbation-theory expansion from Condon and Shortley,[19] we have

$$W_F^{(3)}(^3P_2)=\frac{|\langle ^3P_2|\mathcal{H}_h|^3P_1\rangle|^2}{[W(^3P_2)-W(^3P_1)]^2}[\langle ^3P_1|\mathcal{H}_h|^3P_1\rangle-\langle ^3P_2|\mathcal{H}_h|^3P_2\rangle]+\frac{|\langle ^3P_2|\mathcal{H}_h|^3P_0\rangle|^2}{[W(^3P_2)-W(^3P_0)]^2}$$
$$\times[\langle ^3P_0|\mathcal{H}_h|^3P_0\rangle-\langle ^3P_2|\mathcal{H}_h|^3P_2\rangle]+\frac{2\langle ^3P_2|\mathcal{H}_h|^3P_1\rangle\langle ^3P_2|\mathcal{H}_h|_3P_0\rangle\langle ^3P_1|\mathcal{H}_h|^3P_0\rangle}{[W(^3P_2)-W(^3P_1)][W(^3P_2)-W(^3P_0)]},\quad\text{(A1)}$$

$$W_F^{(3)}(^3P_1)=\frac{|\langle ^3P_1|\mathcal{H}_h|^3P_2\rangle|^2}{[W(^3P_1)-W(^3P_2)]^2}[\langle ^3P_2|\mathcal{H}_h|^3P_2\rangle-\langle ^3P_1|\mathcal{H}_h|^3P_1\rangle]+\frac{|\langle ^3P_1|\mathcal{H}_h|^3P_0\rangle|^2}{[W(^3P_1)-W(^3P_0)]^2}[\langle ^3P_0|\mathcal{H}_h|^3P_0\rangle$$
$$-\langle ^3P_1|\mathcal{H}_h|^3P_1\rangle]+\frac{2\langle ^3P_1|\mathcal{H}_h|^3P_2\rangle\langle ^3P_1|\mathcal{H}_h|^3P_0\rangle\langle ^3P_2|\mathcal{H}_h|^3P_0\rangle}{[W(^3P_1)-W(^3P_2)][W(^3P_1)-W(^3P_0)]}.\quad\text{(A2)}$$

[14] R. G. Barnes and W. V. Smith, Phys. Rev. **93**, 95 (1954).
[15] R. M. Sternheimer, Phys. Rev. **95**, 736 (1954); **105**, 158 (1957).
[16] A. Lurio and A. G. Blachman, Bull. Am. Phys. Soc. **5**, 344 (1960); A. Lurio and A. G. Blachman, *ibid.* **6**, 142 (1961).
[16a] R. M. Sternheimer (private communication); see also Phys. Rev. **84**, 244 (1951).
[17] P. D. Kunz, Phys. Rev. **128**, 1343 (1962).
[18] J. Hiura and I. Shimodaya, Progr. Theoret. Phys. (Kyoto) **30**, 585 (1963).
[19] E. U. Condon and G. H. Shortley, *The Theory of Atomic Spectra* (Cambridge University Press, London, 1951), pp. 34–35.

After evaluation of the appropriate matrix elements we obtain, for the case where $I=\frac{3}{2}$,

$$W_{7/2}{}^{(3)}({}^3P_2)=0,$$

$$W_{5/2}{}^{(3)}({}^3P_2)=\frac{(63/64)\{A'-\frac{1}{3}B'\}^2}{W_{12}{}^2}\{\tfrac{1}{2}A({}^3P_2)+\tfrac{5}{8}B({}^3P_2)+\tfrac{3}{2}A({}^3P_1)+\tfrac{1}{4}B({}^3P_1)\},$$

$$W_{3/2}{}^{(3)}({}^3P_2)=\frac{\frac{3}{4}\{A'+\frac{1}{2}B'\}^2}{W_{12}{}^2}\{-A({}^3P_1)-B({}^3P_1)+3A({}^3P_2)\}+\frac{1}{W_{02}{}^2}\{\tfrac{5}{8}[\eta B({}^3P_2)]^2\}\{3A({}^3P_2)\}$$

$$-\frac{(15/16)\sqrt{2}}{(W_{12})(W_{20})}\{\eta B({}^3P_2)\}\{A'+\tfrac{1}{2}B'\}\{A''\},$$

and

$$W_{1/2}{}^{(3)}({}^3P_2)=\frac{(15/64)\{A'+B'\}^2}{W_{12}{}^2}\left\{\frac{9}{2}A({}^3P_2)-\frac{7}{8}B({}^3P_2)-\frac{5}{2}A({}^3P_1)+\frac{5}{4}B({}^3P_1)\right\},$$

$$W_{5/2}{}^{(3)}({}^3P_1)=-W_{5/2}{}^{(3)}({}^3P_2), \tag{A3}$$

$$W_{3/2}{}^{(3)}({}^3P_1)=\frac{\frac{3}{4}\{A'+\frac{1}{2}B'\}^2}{W_{21}{}^2}\{A({}^3P_1)+B({}^3P_1)-3A({}^3P_2)\}+\frac{(15/16)\{A''\}^2}{W_{01}{}^2}$$

$$\times\{A({}^3P_1)+B({}^3P_1)\}-\frac{(15/16)\sqrt{2}}{(W_{01})(W_{12})}\{\eta B({}^3P_2)\}\{A'+\tfrac{1}{2}B'\}\{A''\},$$

and

$$W_{1/2}{}^{(3)}({}^3P_1)=-W_{1/2}{}^{(3)}({}^3P_2), \tag{A4}$$

where

$$A'\equiv c_1a_s-c_1a_{3/2}-\tfrac{5}{8}\sqrt{2}c_2\xi a_{3/2},$$

$$B'\equiv(c_1+\sqrt{2}c_2\eta)b_{3/2},$$

and

$$A''\equiv c_2a_s-c_2a_{1/2}-\tfrac{5}{8}\sqrt{2}c_1\xi a_{3/2}, \tag{A5}$$

and the fine-structure separations are

$$W_{12}\equiv W^{(0)}({}^3P_1)-W^{(0)}({}^3P_2)=-W_{21},$$

$$W_{02}\equiv W^{(0)}({}^3P_0)-W^{(0)}({}^3P_2)=-W_{20},$$

and

$$W_{01}\equiv W^{(0)}({}^3P_0)-W^{(0)}({}^3P_1). \tag{A6}$$

In the above formulas, perturbations between either ^3P state and the $^1P_1$ state have been ignored because $[W(^1P_1)-W(^3P_J)]/[W(^3P_2)-W(^3P_0)]\sim10^4$ for Be.

APPENDIX B. ESTIMATE OF INTERMEDIATE COUPLING COEFFICIENTS c_1 AND c_2

In LMN it is shown that, in terms of the lifetimes of the $^1P_1$ and $^3P_1$ states, one has

$$\frac{\beta^2}{\alpha^2}=\frac{\tau(^1P_1)}{\tau(^3P_1)}\frac{\lambda^3(^3P_1-{}^1S_0)}{\lambda^3(^1P_1-{}^1S_0)}, \tag{B1}$$

where $c_1=\alpha\sqrt{\frac{1}{3}}+\beta\sqrt{\frac{2}{3}}$ and $c_2=\alpha\sqrt{\frac{2}{3}}-\beta\sqrt{\frac{1}{3}}$. The $^1P_1$ state lifetime can be reliably estimated from our knowledge of the oscillator strengths f of the other Group II $^1P_1$ states. Excluding Hg, the oscillator strengths of all the other $(^1P_1-{}^1S_0)$ transitions lie between 1.42 and 1.92. The Bates and Damgaard[20] value of $f(2349\text{ Å})$ is 1.55. A number of other theoretical calculations have appeared in the literature and are consistent with these values.[21] We will choose, therefore, the value $f(2349\text{ Å})=1.65\pm0.2$ to obtain the estimate $\tau(^1P_1)\cong1.50\times10^{-9}$ sec. We can estimate the value of $\tau(^3P_1)$ from the plot in Fig. 10. This gives for Be, $10^{-3}\text{ sec}\leq\tau(^3P_1)\leq10^{-2}$ sec. The value of $\tau(^3P_1)$ cannot be less than $\sim3\times10^{-4}$ sec; otherwise the intensities of the observed transitions in the $^3P_1$ state would be much less than those observed in the $^3P_2$ state. We find the intensities to be approximately equal. In

TABLE VI. Values of the coupling coefficients for $\tau(^3P_1)$ lying between 10^{-3} sec and ∞, based on Eq. (B1).[a]

$\tau(^3P_1)$ (sec)	β^2	β	c_1	c_2
10^{-3}	1.12×10^{-5}	-3.35×10^{-3}	0.57462	0.81843
3×10^{-3}	3.74×10^{-6}	-1.94×10^{-3}	0.57577	0.81762
10^{-2}	1.12×10^{-6}	-1.06×10^{-3}	0.57649	0.81711
10^{-1}	1.12×10^{-7}	-3.35×10^{-4}	0.57708	0.81669
∞	0	0	0.57735	0.81650

[a] For all calculations $\tau(^1P_1)=1.55\times10^{-9}$ sec.

[20] D. R. Bates and A. Damgaard, Phil. Trans. Roy. Soc. London **A242**, 101 (1949).

[21] H. P. Kelly, Phys. Rev. **136**, B896 (1964); H. Pfennig, R. Steele and E. Trefftz, J. Quant. Spectr. Radiative Transfer **5**, 535 (1965).

Table VI we list the values of c_1 and c_2 for $\tau(^3P_1)$ lying between 10^{-3} sec and ∞.

One may also estimate c_1 and c_2 from the fine structure. The theory of Wolfe[22] does not apply to Be since spin-spin and spin-other-orbit interactions are large. Araki's[23] calculation of the fine structure of the alkaline earths, however, does apply, and in terms of his notation we have

$$\beta^2=\frac{l(l+1)(Z-\sigma+\zeta_{n_0 0,nl})^2}{4K^2}=\frac{(Z-\sigma+\zeta_{n_0 0,nl})^2}{2K^2}, \qquad \text{(B2)}$$

where β^2 is the same as in Eq. (B1) and we have taken $\alpha\cong 1$. By fitting his theoretical expression to the observed $^1P_1$, $^3P_{2,1,0}$ fine structure, we obtain $Z-\sigma+\zeta_{n_0 0,nl}=1.20$ cm^{-1}, $K=10\,293$ cm^{-1}, and $\beta^2=6.77\times10^{-9}$. This value of β implies $\tau(^3P_1)\cong 1.6$ sec for $\tau(^1P_1)=1.50\times10^{-9}$ sec. Bozman[24] *et al.* have observed the intercombination line $(^1S_0-{}^3P_1)$ and have made a crude estimate of the intensity ratio $I_{2349}/I_{4549}=3\times10^7$, from which one obtains $\tau(^3P_1)/\tau(^1P_1)=5.5\times10^9$ or $\tau(^3P_1)\cong 8$ sec. We can summarize the discussion by saying only that $\tau(^3P_1)\geq 10^{-3}$ sec.

APPENDIX C. HYPERFINE AND ZEEMAN MATRIX ELEMENTS FOR AN *sp* CONFIGURATION IN INTERMEDIATE COUPLING WITH $I=\frac{3}{2}$

In order to compute the energy levels at intermediate magnetic fields one must diagonalize the energy matrix. The elements of this matrix are conveniently calculated in the F, m_F representation by making use of the results of LMN. In all calculations we have adopted the correlation of I, J, F, m_F and S, L, J, m_J to j_1, j_2, J, m as standard. Since all elements are diagonal in m_F, there are eight matrices to diagonalize, one for each m_F value. To indicate the nature of the problem we give the nonvanishing elements for the $m_F=\pm\frac{3}{2}$ matrices, where the elements are arranged in order of decreasing J and F. With the wave function notation $|JFm_F\rangle$, the ordering is $|2,\frac{7}{2},\frac{3}{2}\rangle$, $|2,\frac{5}{2},\frac{3}{2}\rangle$, $|2,\frac{3}{2},\frac{3}{2}\rangle$, $|1,\frac{5}{2},\frac{3}{2}\rangle$, $|1,\frac{3}{2},\frac{3}{2}\rangle$, $|0,\frac{3}{2},\frac{3}{2}\rangle$, and, for example, $\mathcal{H}_{23}=\langle 2,\frac{5}{2},\frac{3}{2}|\mathcal{H}|2,\frac{3}{2},\frac{3}{2}\rangle$. Here

$$\mathcal{H}=\mathcal{H}_{\rm fs}+\mathcal{H}_{\rm dipole}+\mathcal{H}_{\rm quadrupole}+\mathcal{H}_{\rm Zeeman}$$

and interactions between the ^3P_J levels and the $^1P_1$ level have been ignored. Thus we have:

$$\mathcal{H}_{11}=W(^3P_2)+\frac{3}{4}a_s+\frac{9}{4}a_{3/2}+\frac{1}{4}b_{3/2}\pm\left[\frac{6}{7}g_J'(^3P_2)+\frac{9}{14}g_I\right]\mu_0 H,$$

$$\mathcal{H}_{12}=\mathcal{H}_{21}=-\frac{2\sqrt{5}}{7}[g_J'(^3P_2)-g_I]\mu_0 H,$$

$$\mathcal{H}_{14}=\mathcal{H}_{41}=(c_1\sqrt{\tfrac{1}{3}}+c_2\sqrt{\tfrac{2}{3}})\left(\frac{5}{21}\right)^{1/2}(g_S-g_L)\mu_0 H,$$

$$\mathcal{H}_{22}=W(^3P_2)-\tfrac{1}{8}a_s-\tfrac{3}{8}a_{3/2}-\tfrac{5}{8}b_{3/2}\pm\left[\frac{33}{35}g_J'(^3P_2)+\frac{39}{70}g_I\right]\mu_0 H,$$

$$\mathcal{H}_{23}=\mathcal{H}_{32}=-\frac{\sqrt{14}}{5}[g_J'(^3P_2)-g_I]\mu_0 H,$$

$$\mathcal{H}_{24}=\mathcal{H}_{42}=\frac{3\sqrt{7}}{8}\left[c_1a_s-\left(c_1+c_2\frac{5\sqrt{2}}{8}\xi\right)a_{3/2}\right]-\frac{\sqrt{7}}{8}(c_1+c_2\sqrt{2}\eta)b_{3/2}\pm(c_1\sqrt{\tfrac{1}{3}}+c_2\sqrt{\tfrac{2}{3}})\frac{3}{10}\left(\frac{3}{7}\right)^{1/2}(g_S-g_L)\mu_0 H,$$

$$\mathcal{H}_{25}=\mathcal{H}_{52}=(c_1\sqrt{\tfrac{1}{3}}+c_2\sqrt{\tfrac{2}{3}})\tfrac{1}{5}(\tfrac{7}{2})^{1/2}(g_S-g_L)\mu_0 H,$$

$$\mathcal{H}_{33}=W(^3P_2)-\frac{3}{4}a_s-\frac{9}{4}a_{3/2}\pm\left[\frac{6}{5}g_J'(^3P_2)+\frac{3}{10}g_I\right]\mu_0 H,$$

$$\mathcal{H}_{34}=\mathcal{H}_{43}=-(c_1\sqrt{\tfrac{1}{3}}+c_2\sqrt{\tfrac{2}{3}})\tfrac{1}{10}(\tfrac{2}{3})^{1/2}(g_S-g_L)\mu_0 H,$$

$$\mathcal{H}_{35}=\mathcal{H}_{53}=\frac{\sqrt{3}}{2}\left[c_1a_s-\left(c_1+c_2\frac{5\sqrt{2}}{8}\xi\right)a_{3/2}\right]+\frac{\sqrt{3}}{4}(c_1+c_2\sqrt{2}\eta)b_{3/2}\pm(c_1\sqrt{\tfrac{1}{3}}+c_2\sqrt{\tfrac{2}{3}})\tfrac{2}{5}(g_S-g_L)\mu_0 H,$$

$$\mathcal{H}_{36}=\mathcal{H}_{63}=\tfrac{1}{2}(\tfrac{5}{2})^{1/2}\eta b_{3/2},$$

[22] H. C. Wolfe, Phys. Rev. **41**, 443 (1932).
[23] G. Araki, Proc. Phys. Math. Soc. Japan **19**, 592 (1937).
[24] W. R. Bozman, C. H. Corliss, W. F. Meggers and R. E. Trees, J. Res. Natl. Bur. Std. **50**, 131 (1953).

$$\mathcal{H}_{44}=W(^3P_1)+\frac{3}{4}\left(c_2^2-\frac{c_1^2}{2}\right)a_s+\frac{15}{8}\left(c_1^2-c_1c_2\frac{\sqrt{2}}{4}\xi\right)a_{3/2}+\frac{3}{4}c_2^2a_{1/2}+\frac{1}{4}\left(\frac{c_1^2}{2}-c_1c_2\sqrt{2}\eta\right)b_{3/2}\pm\left[\frac{3}{5}g_J'(^3P_1)+\frac{9}{10}g_I\right]\mu_0H,$$

$$\mathcal{H}_{45}=\mathcal{H}_{54}=-\frac{\sqrt{6}}{5}[g_J'(^3P_1)-g_I]\mu_0H,$$

$$\mathcal{H}_{46}=\mathcal{H}_{64}=\left(c_1\sqrt{\frac{1}{3}}+c_2\sqrt{\frac{2}{3}}\right)\frac{2}{5}\left(\frac{5}{3}\right)^{1/2}(g_S-g_L)\mu_0H,$$

$$\mathcal{H}_{55}=W(^3P_1)-\frac{1}{2}\left(c_2^2-\frac{c_1^2}{2}\right)a_s-\frac{5}{4}\left(c_1^2-c_1c_2\frac{\sqrt{2}}{4}\xi\right)a_{3/2}-\frac{c_2^2}{2}a_{1/2}-\left(\frac{c_1^2}{2}-c_1c_2\sqrt{2}\eta\right)b_{3/2}\pm\left[\frac{2}{5}g_J'(^3P_1)+\frac{11}{10}g_I\right]\mu_0H,$$

$$\mathcal{H}_{56}=\mathcal{H}_{65}=\frac{\sqrt{15}}{4}\left[c_2(a_s-a_{1/2})-c_1\frac{5\sqrt{2}}{8}\xi a_{3/2}\right]\pm(c_1\sqrt{\tfrac{1}{3}}+c_2\sqrt{\tfrac{2}{3}})(\tfrac{2}{5})^{1/2}(g_S-g_L)\mu_0H,$$

$$\mathcal{H}_{66}=W(^3P_0)\pm\tfrac{3}{2}g_I\mu_0H,$$

where

$$W(^3P_J)=\text{the fine-structure energy},$$
$$g_J'(^3P_2)=g_J(^3P_2{}^0);$$

superscript (0) indicates a pure Russell-Saunders state,

$$g_J'(^3P_1)=(c_1\sqrt{\tfrac{1}{3}}+c_2\sqrt{\tfrac{2}{3}})^2g_J(^3P_1{}^0)+(c_1\sqrt{\tfrac{2}{3}}-c_2\sqrt{\tfrac{1}{3}})^2g_J(^1P_1{}^0),$$

and

$$g_J(^{2S+1}P_J{}^0)=g_L\frac{J(J+1)+L(L+1)-S(S+1)}{2J(J+1)}+g_S\frac{J(J+1)+S(S+1)-L(L+1)}{2J(J+1)}.$$